Dual Source Dual-Energy Computed Tomography of Acute Myocardial Infarction

Correlation With Histopathologic Findings in a Canine Model

Long-Jiang Zhang, MD, Jin Peng, MS,† Sheng-Yong Wu, MD,‡ Benjamin M. Yeh, MD,§ Chang-Sheng Zhou, Bachelor,* and Guang-Ming Lu, MD**

Purpose: To evaluate the feasibility and value of dual-energy computed tomography myocardial iodine maps in the diagnosis of acute myocardial infarction.

Materials and Methods: In 6 dogs, arterial-phase myocardial dual-energy computed tomography imaging were performed 1 day prior to and 3 hours after the surgical ligation of the left anterior descending artery to generate 100 kVp, 140 kVp, average weighted images, and dual energy myocardial iodine maps. For each of the 17 segments of the left ventricle (LV, 102 total segments), the presence or absence myocardial infarction was determined by histopathology and correlated to blinded reader determination of infarcted and noninfarcted myocardium at computed tomography (CT). Statistical analysis for diagnostic accuracy of aforementioned techniques and inter-reader agreement was performed.

Results: The LV myocardial contrast enhancement at the average weighted images and iodine maps were uniform in all 6 dogs before surgery. Following anterior descending artery ligation, histopathology showed 40 infarcted left ventricular segments and 62 noninfarcted segments. For the postligation CT scans, 100 kVp, 140 kVp, average weighted images, and myocardial iodine maps showed 33, 28, 33, 34 infarcted segments and 53, 56, 56, 52 noninfarcted segments for both readers; corresponding to per-segment sensitivities of 83%, 70%, 80%, 92% and specificities of 85%, 90%, 92%, 80% for detecting myocardial infarction. No statistical difference was found for diagnostic accuracy of 100 kV, 140 kV, weighted average images, and iodine maps to detect myocardial infarct segments (all $P > 0.05$ for both readers). Good inter-reader agreement was seen for myocardial infarct detection using iodine maps ($\kappa = 0.80$).

Conclusions: Myocardial single- and dual-energy CT imaging shows high per-segment sensitivity and moderate specificity for detecting acute myocardial infarction in a canine model with histopathology as the standard of reference.

Key Words: dual-source CT, dual energy, myocardial infarction

(*Invest Radiol* 2010;45: 290–297)

Refinements in computed tomographic (CT) technology, including faster gantry rotations, multidetector arrays, and dual-source scanners, have led to the proposal of CT angiography (CTA) as a promising alternative to conventional coronary angiography for the diagnosis of coronary artery disease in selected patients. Recent studies have documented the high sensitivity (73%–100%) and specificity (90%–97%) of dual-source CT (DSCT) angiography for the detection of coronary artery stenoses, with conventional angiography as standard of reference.[1,2] However, conventional coronary CTA focuses on anatomic findings and does not assess the hemodynamic relevance of a given coronary lesion on myocardial perfusion.

Research on visualizing myocardial infarction by contrast enhancement at CT dates back to the 1980s.[3] In experimental and clinical studies, perfusion CT techniques have been used to detect hemodynamic derangements of infarcted myocardium.[4–8] However, even with improved multidetector CT technology, the evaluation of myocardial perfusion at CT has inherent limitations, including limited coverage area, high radiation dose, and additional scans required to evaluate coronary artery morphology. The recent development of DSCT scanners, whereby 2 orthogonally mounted detectors and tubes arrays can simultaneously acquire images at different tube potentials, allows for dual-energy CT (DECT) acquisitions without patient motion registration artifact.[9] Interest in dual-source or dual-energy CT is rising, and this modality has been used to improve the detection of pulmonary embolism[10–13] and vascular disease,[14–18] characterize the composition of kidney stones,[19–22] and reduce the radiation dose needed to assess for endoleak after endovascular repair of aortic aneurysms.[23,24] For dual-source dual-energy scanning, one tube can be set at a peak tube voltage of 100 kVp and the other at 140 kVp, and the resultant datasets can be reformatted to extract maps of intramyocardial iodine contrast-material content as well as separate CT coronary angiograms from the fused average weighted images.[25–29] Although currently published studies show that a single contrast-enhanced DECT coronary angiogram examination permits the assessment of myocardial infarction and coronary artery anatomy and stenoses, these studies have not included histopathologic proof of myocardial infarction as a reference standard. Clearly the diagnostic accuracy of DECT for the detection of myocardial infarction needs to be validated against histopathology and such a standard of reference is most ethically obtained using an animal model. Therefore, the purpose of our study was to demonstrate the feasibility and value of DECT for detection of myocardial infarction in an experimental canine model.

MATERIALS AND METHODS

Animal Model

Our study protocol was approved by our institutional animal experimental committee and performed according to Chinese animal care guidelines. Studies were performed in 6 healthy adult dogs (Jinling Hospital Laboratories, Nanjing, Jiangsu, China) each weighing approximately 15 kg. After intramuscular induction of anesthesia with ketamine hydrochloride injection (Jiangsu Hengrui Medicine Co, Ltd, Lianyungang, China), the animals were intubated. Anesthesia was maintained by means of a mechanical respirator (VIP Gold-Bird, Viasys Respiratory Care Inc, CA) with 2% to 3%

Received September 12, 2009, and accepted for publication, after revision, November 30, 2009.

From the *Department of Medical Imaging, Jinling Hospital, Clinical School of Medical College, Nanjing University, Jiangsu, China; and †Department of Radiology, Bailu Hospital, Siming District, Xiamen, Fujian Province, China; and ‡Medical Imaging Institute of Tianjin, Tianjin, China; and §Department of Radiology and Biomedical Imaging, University of California, San Francisco, CA.

Reprints: Guang-Ming Lu, Department of Medical Imaging, Jinling Hospital, Clinical School of Medical College, Nanjing University, Zhongshan East Rd 305, Xuanwu District, Nanjing, Jiangsu Province 200012, China. E-mail: cjr.luguangming@vip.163.com.

ISSN: 0020-9996/10/4506-0290

nitrous oxide, 1% oxygen, and 2% to 3% isoflurane (Shanghai Yapei Medicine Co, Ltd., Shanghai, China) for both surgery and CT imaging. Mechanical respiratory tidal volumes were 8 to 12 mL/kg with a frequency of 20 strokes per minute. Following midline sternotomy and pericardiotomy, a ligature was placed around the mid segment of the left anterior descending coronary artery (LAD). Afterward, the pericardium and sternotomy were closed. During the acquisition of dual-energy CT dataset, esmolol hydrochloride injection (Nanjing Hencer Pharmacy, Nanjing, China) was administrated continuously at a rate of 100 to 150 g/min for heart rate reduction. All surgeries were performed by an experienced animal technician (J. P.).

Scan Protocols

All CT examinations were performed on a dual-source CT scanner (Somatom Definition, Siemens Medical Solutions, Forchheim, Germany). A single contrast-enhanced DECT scan was performed both 1 day before and 3 hours after the ligation of the mid segment of the LAD (experimental procedure shown in Fig. 1). The dogs were positioned in center of the scanner to ensure that the entire thorax was covered by the field-of-view of both the larger and smaller tube detector arrays; the maximum field-of-view of the second (smaller) tube-detector array was 260 mm. A contrast-enhanced CT scan using dual-energy mode was obtained after intravenous administration of 2 mL/kg of iopromide (Ultravist 300 mg I/mL, Bayer Schering Pharma, Berlin, Germany, 2 mL/kg) followed by 30 mL of saline, both delivered at 3.0 mL/s into a posterior limb vein through an 18-gauge catheter. The CT scan was triggered by a bolus tracking technique with the region of interest placed in the root of the aorta, and image acquisition began 3 seconds after the CT attenuation reached a predefined threshold of 100 Hounsfield Units at 100 kVp. The other CT scan parameters were as follows: tube voltages of 100 and 140 kVp and tube currents of 164 and 82 mA for the larger and smaller x-ray tubes, respectively; gantry rotation time of 0.33 seconds, detector collimation of $32 \times 2 \times 0.6$ mm, pitch 0.6, and a field of view 260 mm for both tube-detector arrays. Data were acquired in a craniocaudal direction with simultaneous recording of the dog's electrocardiogram signal to allow for retrospective registration of image reconstruction to the desired cardiac phase. The anatomic range of imaging extended from the level of the carina to just below the dome of the diaphragm. Electrocardiogram-dependent tube-current modulation was used. The mean radiation dose as expressed in volume CT dose index ($CTDI_{vol}$, which is a measure of radiation exposure per slice) and dose length product (DLP, which is a measure of total radiation exposure for the whole series of images. $DLP = CTDI_{vol} \times$ irradiated length) were 31.24 ± 0.04 mGy (range, 31.20–31.27 mGy) and 405.50 ± 32.13 mGy cm (range, 385–470 mGy cm).

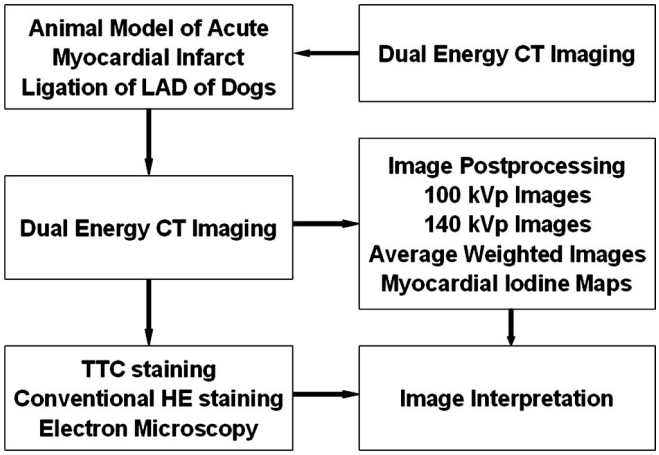

FIGURE 1. Flow chart illustrating the experimental procedures for this study. TTC staining indicates triphenyltetrazolium chloride staining.

Image Reconstruction and Analysis

From the raw spiral projection data of both tubes, images were then automatically reconstructed into 3 image datasets (100 kVp, 140 kVp, and an average weighted image set). The average weighted images were weighted fused images (with 70% contribution from the 140 kVp scan and 30% from the 100 kVp scan) with 1.5 mm slice thickness and 0.5 mm intervals (33% overlap) using the routine dual-energy reconstruction algorithm implemented on the scanner platform. A 100 kVp, 140 kVp, and the average weighted images were used for diagnostic interpretation, respectively. All images were then transferred to a commercially available workstation (Syngommvvp VE23A, Siemens Medical Solutions, Forchheim, Germany) where dedicated cardiac dual energy analysis software (heart perfusion blood volume [PBV]) was used to obtain myocardial "iodine maps" in the short axis, long axis, and 4 chamber views. These iodine maps, which represent the myocardial blood pool, were 16-bit color-coded and then superimposed onto the grayscale anatomic multiplanar reformations of the myocardium. In the workstation color-code scheme ("Hot Body" option) was used, yellow represented the highest amount of iodine; brown represented low iodine; and an absence of color represented absent iodine.

All images were evaluated independently by 2 radiologists (L.-J.Z. and J.P., with 3 and 2 years of experience in DECT interpretation, respectively) who were unaware of the histopathologic findings. The readers viewed the 100 kVp, 140 kVp, and average weighted images to record whether the images were diagnostic to clearly define the anatomic the location of LAD occlusion. The images of the left ventricular (LV) myocardium were then evaluated for acceptability for interpretation, and the presence or absence of myocardial infarction was recorded for each image set for each of the 17 segments of the left ventricle, as described by the American Heart Association 17 segmental model.[30] Using 100 kVp,140 kVp, and the average weighted images, noninfarcted myocardium was defined as having homogeneous enhancement without any areas of hypoattenuation; infarcted myocardium was defined as showing distinct hypoattenuation compared with other segments of myocardium.

Two weeks later, the dual-energy myocardial iodine maps were evaluated independently by 2 radiologists (L.-J.Z. and J.P.) without the help of multiplanar anatomic images. For the DECT-based myocardial iodine maps, noninfarcted myocardium was defined as showing homogeneous high iodine distribution in the myocardium of LV wall (yellow color on the iodine map), whereas infarcted myocardium was defined as showing heterogeneous iodine distribution with segmental diminished or absent iodine (brown or absent color on the iodine maps). Reading in consensus was also performed.

For each dataset (ie, 100 kVp, 140 kVp, average weighted images, and DECT-based myocardial iodine maps), image quality was determined by use of a subjective scale: 1, poor; 2, moderate; 3, good, and 4, excellent. The absence or presence of a perfusion defect was also evaluated for the aforementioned dataset. If a perfusion defect was viewed as presence, perfusion defect severity was graded as transmural (>50%) vs. nontransmural (<50%).[31]

For the average weighted images, the CT numbers were recorded as the mean of at least 2 10 mm^2 circular regions of interest that were manually placed on the myocardium, with care to avoid the edges of the myocardium during end diastole. Similar measurements were made for the source 100 and 140 kVp images. The signal-to-noise ratio (SNR) was calculated as follows: SNR = signal intensity (mean CT number)/noise, for the infarcted and normal myocardium of the LV wall, and LV blood pool.

After image interpretation was complete for all of the scans, both readers rereviewed the average weighted images and DECT-based myocardial iodine maps for LV segments where discrepant results were seen between CT and histopathologic findings (described later). The source of interpretation error, such as beam hardening artifacts from high concentrations of contrast material in the cardiac chambers, cardiac motion, and respiratory motion, for the CT interpretation was then recorded.

Histopathology

Histopathology was regarded as the standard of reference in this study. Immediately after DECT, all dogs were killed and the hearts excised. The myocardium of the left ventricle was cut into 8-mm contiguous slices in the short axis. For viability assessment, the slices were embedded in a solution of 1% triphenyltetrazolium chloride (TTC) and 0.2 mol/L Sörensen's buffer (pH, 7.4) at 37°C for 15 minutes and then fixed in 4% formalin. The slices were photographed with a digital camera, and infarcted segments were recorded. Infarctions were further confirmed with hematoxylin and eosin staining and electron microscopy for each of the 17 segments of the left ventricle for each of the 6 hearts (102 total segments) according to the American Heart Association 17 segmental model.[30]

Statistical Analysis

Statistical analysis was performed using a commercially available statistical package (SPSS version 11.5 SPSS Inc, Chicago, IL). One-way ANOVA was used to compare the mean CT numbers and SNR of the infarcted and noninfarcted myocardium for the 100 kVp, 140 kVp, and average weighted images. Independent sample student *t* tests were used to compare the mean CT numbers for the infarcted and normal myocardium. Using the pathologic results as the standard of reference, the per-segment sensitivity, specificity, positive predictive value, and negative predictive value, and accuracy of 100 kVp, 140 kVp, average weighted images, and DECT-based iodine maps for the detection of myocardial infarction were determined. Mc-Nemar tests were performed for comparison of accuracy of 100kV, 140kV, weighted average images, and iodine maps to detect myocardial infarct segments. Kappa statistics were also calculated to quantify inter-reader variability for the detection of ischemic myocardium using 100 kVp, 140kVp, average weighted images, and DECT-based myocardial iodine maps. Kappa values less than 0.20 were interpreted as poor agreement, 0.21–0.40 as fair agreement, 0.41–0.60 as moderate, 0.61–0.80 as good, and 0.81–1.00 as very good agreement. $P < 0.05$ was regarded as statistically significant.

RESULTS

The numbers and locations of infarcted myocardium visualized at TTC staining are listed in Table 1. Transmural myocardial infarcts were demonstrated by TTC staining for all 6 dogs.

The mean heart rate for the 6 dogs was 116 ± 12 beats per minute (bpm; range, 94–125 bpm). None of the CT image sets were judged to be diagnostic to clearly define the location of coronary artery ligation by CT angiography. However, the image quality of 100 kVp (excellent, n = 2; good, n = 4), 140 kVp (excellent, n = 3; good, n = 3), average weighted images (excellent, n = 2; good, n = 4), and DECT-based myocardial iodine maps (excellent, n = 1; good, n = 4; moderate, n = 1) was acceptable for all 6 dogs in all 17 segments before and after LAD ligation. As shown in Table 2, the

TABLE 1. Location and Numbers of Infarcted Myocardial Segments as Determined by DECT and Pathology (n = 6 Dogs)

	Myocardial Segment																	
Modality	**1**	**2**	**3**	**4**	**5**	**6**	**7**	**8**	**9**	**10**	**11**	**12**	**13**	**14**	**15**	**16**	**17**	**Overall**
DECT imaging																		
Reader 1																		
100 kVp images	3	1	3	1	0	0	6	6	2	0	0	4	6	6	0	5	6	49
140 kVp images	2	1	1	1	0	0	6	5	1	0	0	4	6	5	0	6	6	44
Average weighted images	3	1	2	2	0	0	6	6	1	0	0	4	6	6	0	6	6	49
Iodine maps	2	2	4	1	0	0	6	5	3	0	0	4	6	6	0	6	6	51
Reader 2																		
100 kVp images	4	4	0	1	0	0	6	4	0	0	0	2	6	3	0	6	6	42
140 kVp images	4	2	0	0	0	0	5	1	0	0	0	2	6	3	0	1	6	30
Average weighted images	0	0	0	1	0	0	5	4	0	0	0	4	6	6	0	6	6	38
Iodine maps	0	2	2	1	0	0	6	6	2	0	1	3	6	6	0	6	6	47
Histopathology	0	0	0	0	0	0	6	4	0	0	3	6	6	3	0	6	6	40

The average weighted images were created by a weighted fusion of the 100 and 140 kVp images.

TABLE 2. CT Numbers in Infarcted (n = 40) and Noninfarcted (n = 62) Myocardial Segments as Determined by DECT

	Infarcted Segments		Noninfarcted Segments	
CT Tube Potential	**CT Number (HU)**	**SNR**	**CT Number (HU)**	**SNR**
100 kVp images	36.70 ± 33.74*	2.28 ± 1.22	121.10 ± 28.20	13.38 ± 6.39
140 kVp images	26.35 ± 22.65*	2.98 ± 2.52	115.10 ± 16.56	21.51 ± 7.85
Average weighted images	34.75 ± 16.66*	4.29 ± 3.82	123.38 ± 11.20	22.50 ± 7.24

The average weighted images were created by a weighted fusion of the 100 and 140 kVp images.
*$P < 0.001$ unpaired *t* test for mean CT numbers in the infarcted versus non-infarcted myocardial segments.
SNR indicates signal noise ratio.

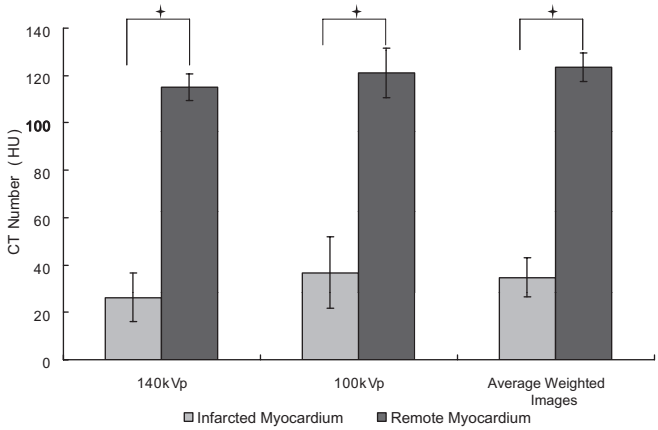

FIGURE 2. Bar-graph of CT numbers (Hounsfield Units) for the infarcted and noninfarcted myocardium at 100 and 140 kVp settings as well as for the average weighted images. For each image set, the mean CT number of the infarcted myocardium was significantly lower than that of noninfarcted myocardium at each CT tube potential setting ($P < 0.001$ for each comparison).

mean CT numbers for the infarcted myocardium were significantly lower than those for noninfarcted myocardium for the 100 kVp, 140 kVp, and average weighted images ($P < 0.001$ for each comparison) (Fig. 2). There was no significant difference in mean SNR for the infarcted and noninfarcted myocardium of the LV wall ($P > 0.05$ for all comparisons).

Before ligation of the LAD, homogeneous attenuation of the LV myocardium was seen in the anatomic images, and homogeneous iodine distribution was seen throughout the LV myocardium in the DECT-based myocardial iodine maps. After ligation of LAD, areas of LV myocardial hypoattenuation were seen in the 100 kVp, 140 kVp, average weighted images, and LV myocardial iodine defects were seen in the DECT-based myocardial iodine maps (Fig. 3). For 100 kVp, 140 kVp, average weighted images, and DECT-based myocardial iodine maps, both readers detected 38 and 47 infarcted segments and 64 and 55 normal segments, respectively (Table 3). Both readers correctly judged 6 dogs having transmural myocardial infarcts. Using the histopathologic findings as the standard of reference, 140 kVp, 100 kVp, average weighted images, and DECT-based myocardial iodine maps correctly diagnosed 35, 34, 35, 35 of 40 infarcted segments and 53, 47, 48, 46 of 62 noninfarcted segments for reader 1; 24, 33, 32, 37 of 40 infarcted segments and 56, 53, 57, 49 of 62 noninfarcted segments for reader 2; corresponding to sensitivities of 88%, 85%, 88%, 88% and specificities of 85%,

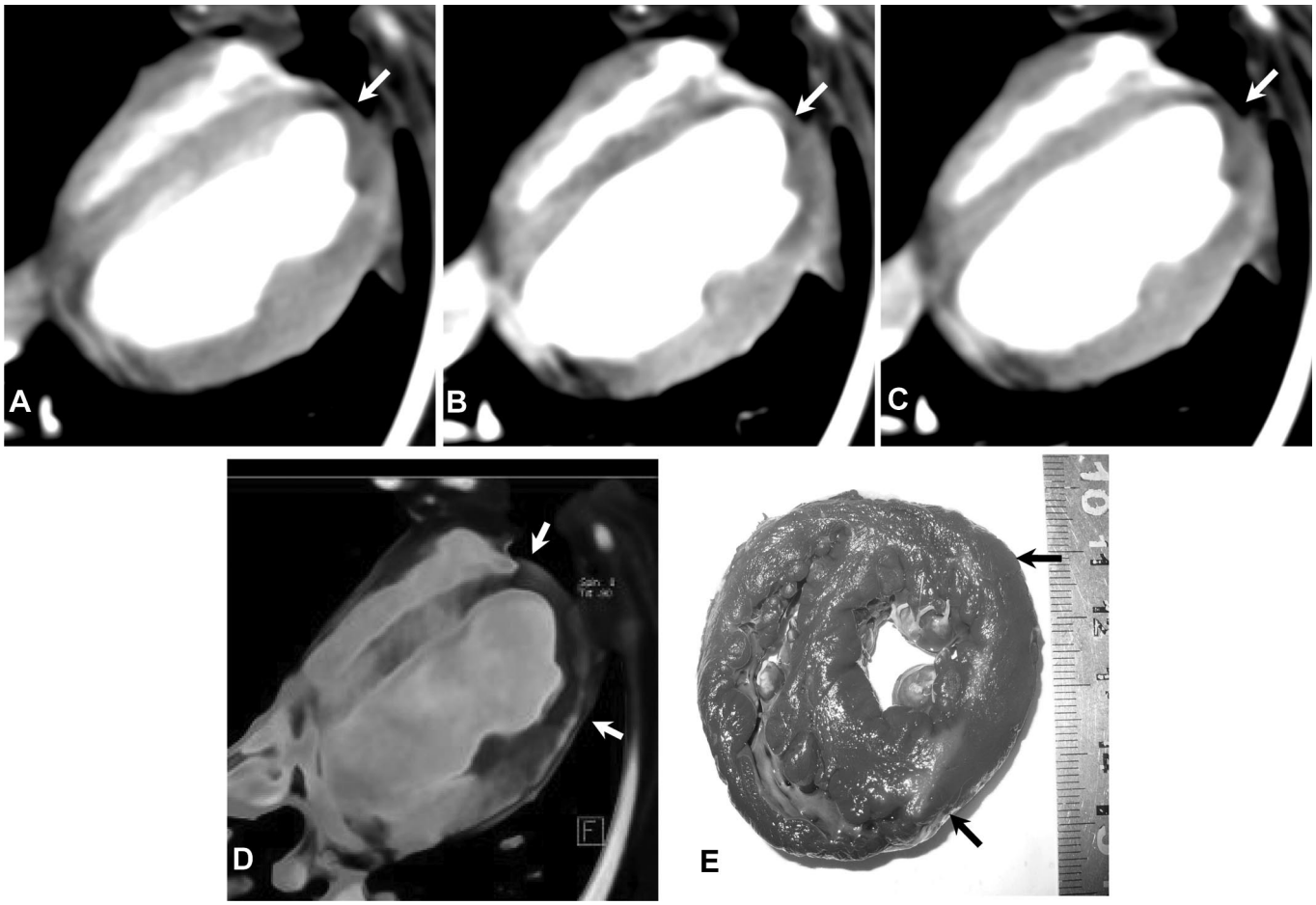

FIGURE 3. A true positive result of DECT-based myocardial iodine maps (A) 140 kVp, (B) 100 kVp, (C) average weighted axial images show myocardial hypoattenuation of the same segment (arrow). D, Myocardial iodine maps show iodine defects in the apex and lateral wall of the left ventricle (arrow). E, TTC staining shows a pale lateral wall of the left ventricle (arrow).

TABLE 3. Diagnostic Accuracy of DECT to Detect Myocardial Infarction

	Results (n)				Detection of Infracted Segments (%)				
Modality	**TP**	**TN**	**FP**	**FN**	**Sensitivity**	**Specificity**	**PPV**	**NPV**	**Accuracy**
Reader 1									
100 kVp images	34	47	15	6	85 (34/40)	76 (47/62)	69 (34/49)	89 (47/53)	79 (81/102)
140 kVp images	35	53	9	5	88 (35/40)	85 (53/62)	80 (35/44)	91 (53/58)	86 (88/102)
Average weighted images	35	48	14	5	88 (35/40)	77 (48/62)	71 (35/49)	91 (48/53)	81 (83/102)
Iodine maps	35	46	16	5	88 (35/40)	74 (46/62)	69 (35/51)	90 (46/51)	79 (81/102)
Reader 2									
100 kVp images	33	53	9	7	83 (33/40)	85 (53/62)	79 (33/42)	88 (53/60)	84 (86/102)
140 kVp images	24	56	6	16	60 (24/40)	90 (56/62)	80 (24/30)	78 (56/72)	78 (80/102)
Average weighted images	32	57	5	8	80 (32/40)	92 (57/62)	86 (32/37)	88 (57/65)	87 (89/102)
Iodine maps	37	49	13	3	93 (37/40)	79 (49/62)	74 (37/50)	94 (49/52)	84 (86/102)
Both readers									
100 kVp images	33	53	9	7	83 (33/40)	85 (53/62)	79 (33/42)	88 (53/60)	84 (86/102)
140 kVp images	28	56	6	12	70 (28/40)	90 (56/62)	82 (28/34)	82 (56/68)	82 (84/102)
Average weighted images	33	56	5	8	80 (33/41)	92 (56/61)	87 (33/38)	88 (56/64)	84 (86/102)
Iodine maps	34	52	13	3	92 (34/37)	80 (52/65)	72 (34/47)	95 (52/55)	87 (89/102)

Average weighted images were created by a weighted fusion of the 100 and 140 kVp images.
TP indicates true positive; FP, false positive; TN, true negative; FN, false negative; PPV, positive predictive value; NPV, negative predictive value.

76%, 77%, 74% for reader 1; sensitivities of 60%, 83%, 80%,93% and specificities of 90%, 85%, 92%, 79% for reader 2, respectively. After reading in consensus, 100 kVp, 140 kVp, average weighted images, and myocardial iodine maps showed 33, 28, 33, 34 infarcted segments and 53, 56, 56, 52 noninfarcted segments for both readers; corresponding to per-segment sensitivities of 83%, 70%, 80%, 92% and specificities of 85%, 90%, 92%, 80% for detecting myocardial infarction. Table 3 illustrated corresponding results and statistical analysis. Figures 3 to 5 presented true-positive, false-positive, and false-negative myocardial infarct images from different dataset. Mc-Nemar tests showed no statistical difference for diagnostic accuracy of 100 kVp, 140 kVp, weighted average images, and iodine maps to detect myocardial infarct segments (all $P > 0.05$ for both readers), indicating dual-energy CT can detect myocardial infarct with the same performance as single energy CT. For inter-reader agreement analysis, Kappa value was 0.46, 0.55, 0.76, and 0.80 for 140 kVp, 100 kVp, average weighted images, and DECT-based myocardial iodine maps (all $P < 0.001$), respectively. After rechecking the corresponding 100 kVp, 140 kVp, average weighted images, and DECT-based myocardial iodine maps, the main causes of interpretation error for DECT-based myocardial iodine maps were judged to be beam-hardening artifacts from high concentrations of contrast material in the left ventricle (n = 12 for reader 1; n = 7 for reader 2), cardiac motion (n = 8 for reader 1; n = 6 for reader 2), and respiratory motion (n = 1 for reader 1; n = 3 for reader 2).

DISCUSSION

Our experimental study found that a single arterial phase contrast-enhanced DECT scan allowed for the detection of histopathologically proven acute myocardial infarction with a high per-segment diagnostic sensitivity of 88% to 93% and moderate specificity of 74% to 79% in a canine model.

In our experimental study, arterial phase contrast enhanced DECT was used to detect hypoattenuated infarcted myocardium because the CT data acquired during the arterial phase have the potential to provide both an anatomic coronary artery evaluation as well as a map of the iodine distribution in the myocardium. Although contrast enhancement is expected to be seen in normal noninfarcted myocardium, delayed wash-in of contrast is expected in infarcted myocardium because of altered microvascular kinetics and reduced functional capillary density with a resultant low mean CT number during the arterial phase compared with normal noninfarcted myocardium.[32] However, infarcted segments may be difficult to identify at CT, especially where the SNR ratio is low or the infarct size is small.

In prior reports, delayed CT scanning at 5 to 15 minutes after the administration of contrast material has been used for the detection of acute myocardial infarcts.[33–36] At the time of a delayed scan, the initial contrast bolus has equilibrated within the intravascular and the extravascular or extracellular space and the mean CT number within healthy myocardium has dropped. However, within myocardial infarcts, there is a relative accumulation of contrast as a result of impaired microvascular circulation and an increased extravascular or extracellular space.[32] This leads to increased attenuation within the infarct zone on delayed images that may be more readily appreciated than hypoattenuation on arterial phase images. However, such delayed imaging techniques have the drawback of requiring an additional scan acquisition that increases the radiation dose to the patient when the same electrocardiographic-gating technique is used for CT coronary angiography acquisitions. Furthermore, the second acquisition prolongs the time required to complete the examination thereby decreasing scanner throughput and potentially places a critical patient in the scanner away from more optimal monitoring outside of the imaging department. It is, therefore, of considerable use to develop a technique to improve the detection of myocardial infarct on the initial CT angiography scan without the need for further acquisitions.[32]

The concept of rapidly obtaining complementary structural and functional CT images of suspected acute myocardial infarctions from a single imaging examination is appealing, and cardiac DECT imaging can potentially meet this demand.[25] The usefulness of this technique for performing contrast-enhanced retrospectively electrocardiographic-gated DSCT angiography for noninvasive coronary artery stenosis detection has recently been demonstrated,[25–29] and our experimental design simulated the clinical setting. In our study, we validate that histopathologically proven myocardial infarctions can be visualized using contrast-enhanced retrospectively electrocardiographic-gated dual-source, DECT technique with a high sen-

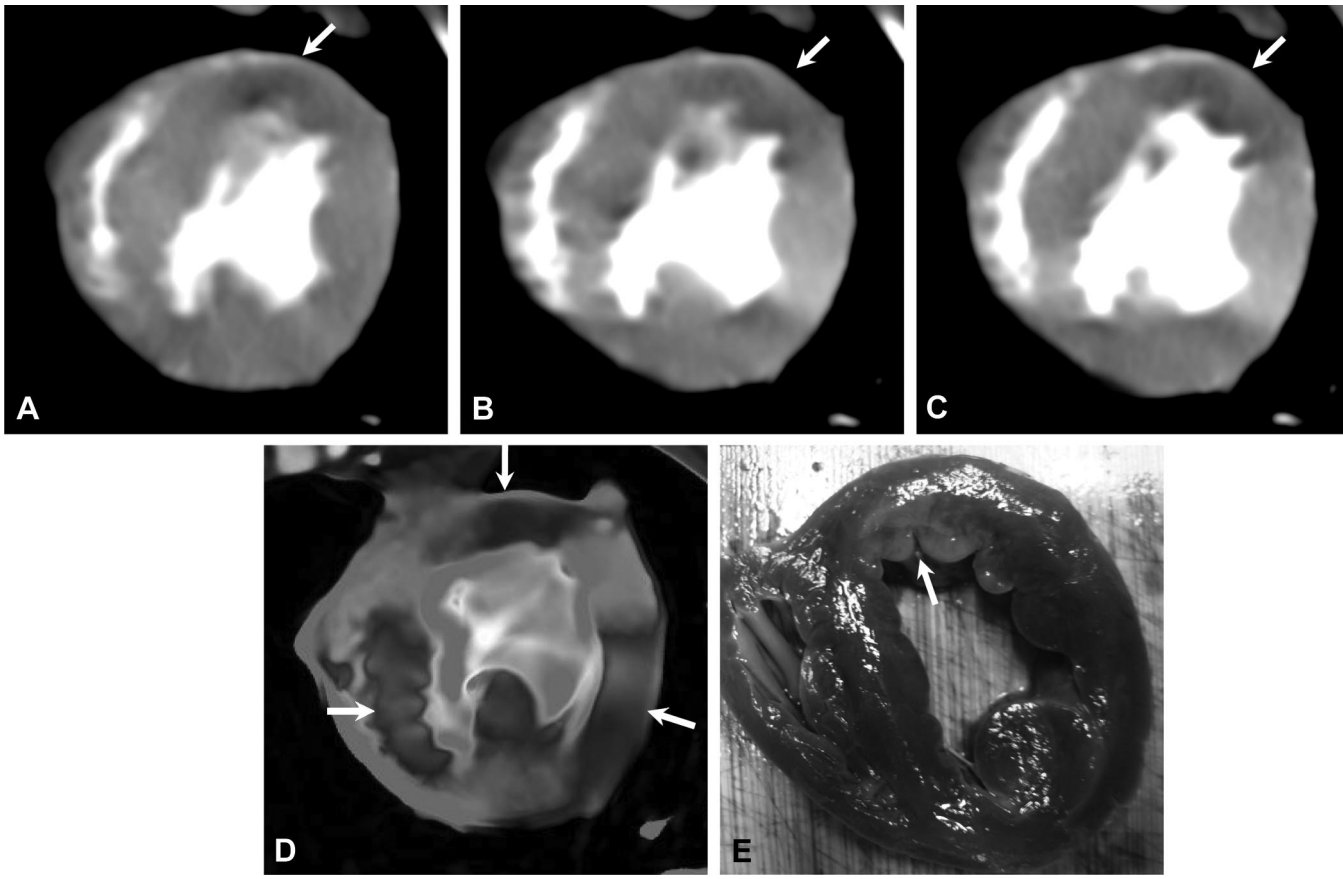

FIGURE 4. False positive results of myocardial infarct on DECT-based myocardial iodine maps (A) 140 kVp, (B) 100 kVp, (C) average weighted short-axis images show myocardial hypoattenuation of segment 7 (arrow). D, Myocardial iodine maps show iodine defects in the segments 7 (top arrow), 9 (left arrow), 11 (right arrow). E, TTC staining shows a pale wall of the left ventricle in segment 7 (arrow).

sitivity of 88% to 93% and a moderate specificity of 74% to 79%. Better inter-reader agreement ($\kappa = 0.80$) was found for myocardial infarct detection using iodine maps than 100 kVp ($\kappa = 0.55$) and 140 kVp ($\kappa = 0.46$) images. Because of the high accuracy of CT for the detection of mycardial infarction, our sample size was not large enough to statistically detect improvements in the diagnosis of myocardial infarction by DECT iodine maps over that of 100 kVp and average-weighted images, but our preliminary results are promising in that they demonstrate the ability of a single arterial phase contrast enhanced DECT scan to detect histopathologically proven acute myocardial infarction. Sixteen false-positive segments and 3 false-negative segments for reader 1 and 13 false-positive segments and 3 false-negative segments for reader 2 were detected by using DECT-based myocardial iodine maps. After rechecking the corresponding anatomic images and DECT-based myocardial iodine maps, we believed the main causes may be the artifacts from high concentration contrast materials of LV and heart motion. In particular, heart motion was a suboptimally controlled component of our examination because the mean heart rate of our small canines was 116 bpm and ranged from 94 to 125 bpm. Rapid heart motion can result in misregistration errors in the CT images that would be less evident in humans where the heart rate is generally slower. Temporal resolution of 165 milliseconds for dual-energy CT cannot freeze heart motion in a larger extent than single-energy dual-source CT (83 milliseconds), which is the major cause of heart motion artifacts in DECT-based myocardial iodine maps. We also noted average weighted images lead to highest SNR as compared with 100 and 140 kVp images, which is not difficult to understand because average weighted images are created by a weighted fusion of the 100 and 140 kVp images, not true 120 kVp images. In our study, the dog with the lowest heart rate of 94 bpm showed excellent quality of DECT-based myocardial iodine maps (Fig. 3), supporting the notion that heart rate influences the quality of DECT-based myocardial iodine maps. The most false-positive results were seen in segments 1 to 3 in the DECT-based myocardial iodine maps, and may have resulted from the misinterpretation of motion or beam hardening artifacts as abnormalities when evaluating DECT-based myocardial iodine maps. This potential pitfall will require further investigation in the clinical setting. The high sensitivity that we found for DECT detection of myocardial infarcts supports the results of prior reports. Ruzsics et al[25] observed that DECT can detect most of the reversible perfusion defects that are only seen during ergometrically or pharmacologically induced hyperemia at 99m-Tc-Sestamibi single photon emission computed tomography (SPECT), and suggested that the excellent sensitivity of DECT was because of the intrinsically higher spatial and contrast resolution of CT in comparison with SPECT.[28] In a following study,[29] they reported DECT showed 92% sensitivity and 93% specificity, with 93% accuracy for detecting any type of myocardial perfusion defects seen on SPECT. These studies demonstrated the value of DECT in the detection of myocardial infarcts by combining the high sensitivity of myocardial iodine maps and high specificity of conventional CT images.

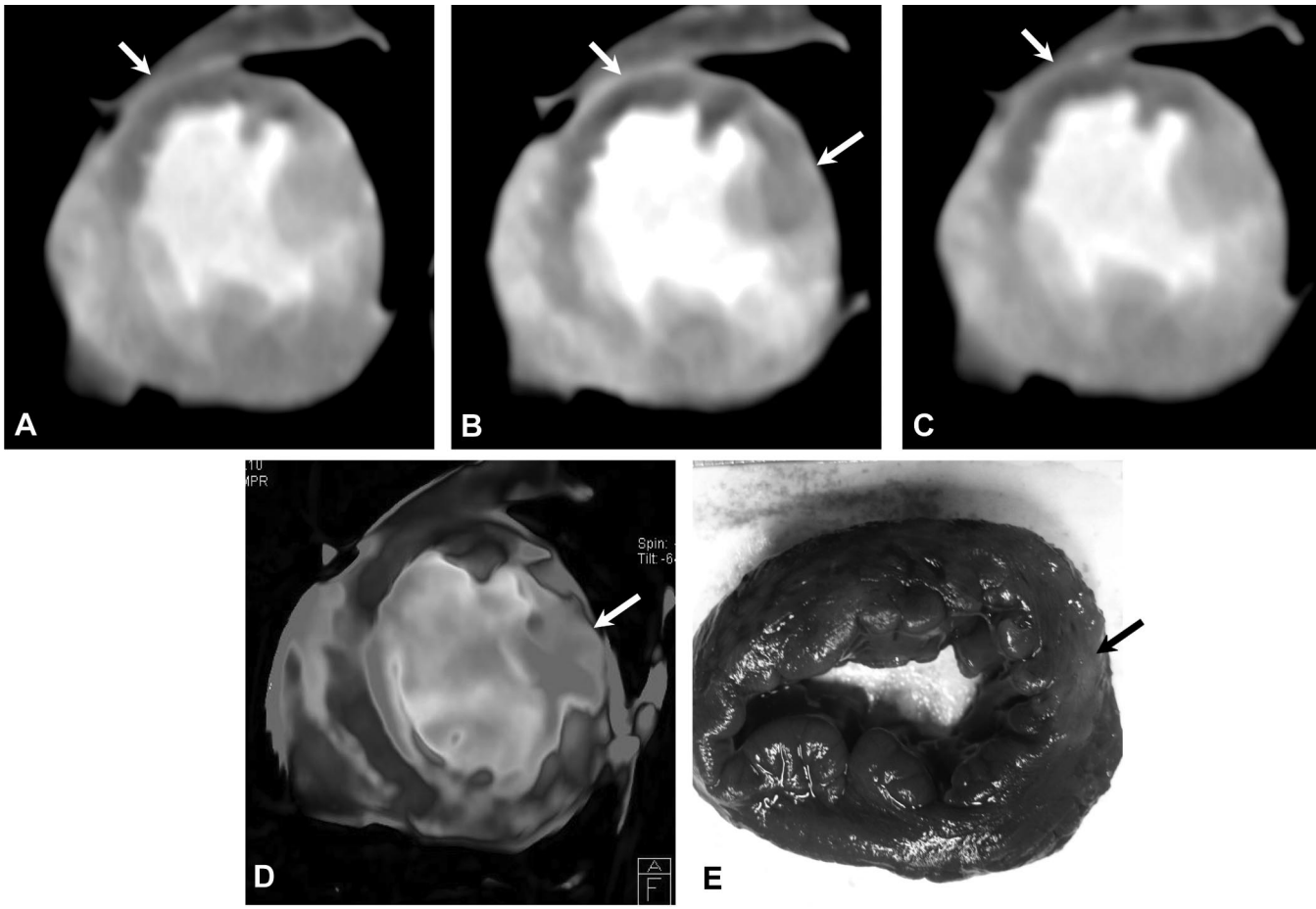

FIGURE 5. False negative result of myocardial infarct on DECT-based myocardial iodine maps (A) 140 kVp, (B) 100 kVp, (C) average weighted short-axis images show myocardial hypoattenuation of segment 7 (left arrow). Note 100 kVp image more clearly shows myocardial hypoattenuation of segment 12 (B, right arrow) than 140 kVp and average weighted images. D, Myocardial iodine maps show iodine defect in the segment 7, however, high iodine content in segment 12 is shown (arrow). E, TTC staining shows pale left ventricle wall in segment 7 and 12 (arrow).

Several limitations should be acknowledged in our study. First, the ligation of only the LAD rather than other coronary arteries in our animals could lead to bias or a systematic error; however, we showed good agreement between the extent of LAD-territory infarction on a per-segment basis in comparison to histopathology. Second, the canine heart rate, which may exceed 180 bpm, is higher than that seen in most clinical patients and degrades the image quality of coronary CT angiography and myocardial CT. In our experimental canine study, even with the intravenous administration of drugs to reduce heart rate to a mean of 116 bpm, we were unable to obtain diagnostic coronary CT angiograms. Clinically, excellent coronary artery and myocardial iodine maps can be routinely obtained when the patient heart rate is less than 70 bpm. Nevertheless, because it would be unethical to obtain histopathologic correlation in most clinical studies, animal models are critical to validate the accuracy of CT techniques. Potentially, the use of animal models with heart rates more comparable to patients, such as a swine model, may improve results.[37,38] Nevertheless, our promising results with a relatively difficult-to-image small canine model helps validate the high accuracy of DECT for clinical myocardial infarction assessment, particularly because no prior DECT study with histopathologic correlation for myocardial infarction has yet been published. Third, comparison of the size of the myocardial infarcts seen at DECT with those seen at histopathology was not performed in our study. However, prior studies demonstrated good correlation for the size of the infarcted myocardium measured by TTC staining and conventional multidetector CT.[36–38] Fourth, our results are limited by small study size (n = 6 dogs). Fifth, because of the novelty of DECT technique, the inexperience of the readers with the appearance of iodine maps may have led to a greater number of artifacts being misclassified as perfusion defects, resulting in underevaluation of ability of DECT to detect myocardial infarct. Sixth, our study did not quantify myocardial blood flow or volume because current heart DECT software cannot provide the quantitative measurements of myocardial blood flow or volume, a limitation can be resolved using a dynamic CT method by George et al.[5]

Notwithstanding these limitations, our experimental study demonstrates that dual-source, single- and dual-energy CT obtained during the arterial phase allows for the detection of acute myocardial infarction with sensitivities of 83% and 92% compared with histopathologic findings as the reference standard. Potentially, with the superior CT images that could be acquired in patients rather than small dogs, a single contrast-enhanced DECT of the heart can simultaneously provide excellent coronary artery angiograms and myocardium perfusion images during the arterial phase without the

need for a separate delayed CT scan to evaluate for the hyperattenuation of the infarcted myocardium.

REFERENCES

1. Weustink AC, Meijboom WB, Mollet NR, et al. Reliable high-speed coronary computed tomography in symptomatic patients. *J Am Coll Cardiol*. 2007;50:786–794.
2. Brodoefel H, Burgstahler C, Tsiflikas I, et al. Dual-source CT: effect of heart rate, heart rate variability, and calcification on image quality and diagnostic accuracy. *Radiology*. 2008;247:346–355.
3. Huber DJ, Lapray JF, Hessel SJ. In vivo evaluation of experimental myocardial infarcts by ungated computed tomography. *Am J Roentgenol.* 1981;136:469–473.
4. Krug KB, Bovenschulte H, Geissler HJ, et al. In vivo measurements of coronary blood flow using 16-slice multidetector spiral computed tomography (MDCT) in a porcine model. *Rofo.* 2009;181:220–229.
5. George RT, Jerosch-Herold M, Silva C, et al. Quantification of myocardial perfusion using dynamic 64-detector computed tomography. *Invest Radiol*. 2007;42:815–822.
6. George RT, Silva C, Cordeiro MA, et al. Multidetector computed tomography myocardial perfusion imaging during adenosine stress. *J Am Coll Cardiol*. 2006;48:153–160.
7. Mahnken AH, Klotz E, Pietsch H, et al. Quantitative whole heart stress perfusion CT imaging as non-invasive assessment of hemodynamics in coronary artery stenosis: preliminary animal experience. *Invest Radiol.* 2010;45:298–305.
8. Bastarrika G, Ramos-Duran L, Rosenblum MA, et al. Adenosine-stress dynamic myocardial CT perfusion imaging: initial clinical experience. *Invest Radiol.* 2010;45:306–313.
9. Johnson TR, Krauss B, Sedlmair M, et al. Material differentiation by dual energy CT: initial experience. *Eur Radiol*. 2007;17:1510–1517.
10. Thieme SF, Becker CR, Hacker M, et al. Dual energy CT for the assessment of lung perfusion—correlation to scintigraphy. *Eur J Radiol*. 2008;68:369–374.
11. Zhang LJ, Zhao YE, Wu SY, et al. Pulmonary embolism detection with dual-energy CT: experimental study of dual-source CT in rabbits. *Radiology*. 2009;252:61–70.
12. Krissak R, Henzler T, Reichert M, et al. Enhanced visualization of lung vessels for diagnosis of pulmonary embolism using dual energy CT angiography. *Invest Radiol.* 2010;45:341–346.
13. Zhang LJ, Chai X, Wu SY, et al. Detection of pulmonary embolism by dual energy CT: correlation with perfusion scintigraphy and pathohistological findings in rabbits. *Eur Radiol*. 2009;19:2844–2854.
14. Tran DN, Straka M, Roos JE, et al. Dual-energy CT discrimination of iodine and calcium: experimental results and implications for lower extremity CT angiography. *Acad Radiol*. 2009;16:160–171.
15. Watanabe Y, Uotani K, Nakazawa T, et al. Dual-energy direct bone removal CT angiography for evaluation of intracranial aneurysm or stenosis: comparison with conventional digital subtraction angiography. *Eur Radiol*. 2009;19:1019–1024.
16. Lell MM, Kramer M, Klotz E, et al. Carotid computed tomography angiography with automated bone suppression: a comparative study between dual energy and bone subtraction techniques. *Invest Radiol*. 2009;44:322–328.
17. Sommer WH, Johnson TR, Becker CR, et al. The value of dual-energy bone removal in maximum intensity projections of lower extremity computed tomography angiography. *Invest Radiol*. 2009;44:285–292.
18. Behrendt FF, Schmidt B, Plumhans C, et al. Image fusion in dual energy computed tomography: effect on contrast enhancement, signal-to-noise ratio and image quality in computed tomography angiography. *Invest Radiol*. 2009;44:1–6.
19. Takahashi N, Hartman RP, Vrtiska TJ, et al. Dual-energy CT iodine-subtraction virtual unenhanced technique to detect urinary stones in an iodine-filled collecting system: a phantom study. *Am J Roentgenol*. 2008;190:1169–1173.
20. Boll DT, Patil NA, Paulson EK, et al. Renal stone assessment with dual-energy multidetector CT and advanced postprocessing techniques: improved characterization of renal stone composition—pilot study. *Radiology*. 2009;250:813–820.
21. Graser A, Johnson TR, Bader M, et al. Dual energy CT characterization of urinary calculi: initial in vitro and clinical experience. *Invest Radiol*. 2008;43:112–119.
22. Scheffel H, Stolzmann P, Frauenfelder T, et al. Dual-energy contrast-enhanced computed tomography for the detection of urinary stone disease. *Invest Radiol*. 2007;42:823–829.
23. Stolzmann P, Frauenfelder T, Pfammatter T, et al. Endoleaks after endovascular abdominal aortic aneurysm repair: detection with dual-energy dual-source CT. *Radiology*. 2008;249:682–691.
24. Chandarana H, Godoy MC, Vlahos I, et al. Abdominal aorta: evaluation with dual-source dual-energy multidetector CT after endovascular repair of aneurysms—initial observations. *Radiology*. 2008;249:692–700.
25. Ruzsics B, Lee H, Zwerner PL, et al. Dual-energy CT of the heart for diagnosing coronary artery stenosis and myocardial ischemia—initial experience. *Eur Radiol*. 2008;18:2414–2424.
26. Ruzsics B, Lee H, Powers ER, et al. Correlation with single-photon emission computed tomography myocardial ischemia diagnosed by dual-energy computed tomography. *Circulation*. 2008;117:1244–1245.
27. Ruzsics B, Chiaramida SA, Schoepf UJ. Images in cardiology: dual-energy computed tomography imaging of myocardial infarction. *Heart*. 2009;95:180.
28. Schwarz F, Ruzsics B, Schoepf UJ, et al. Dual-energy CT of the heart—principles and protocols. *Eur J Radiol*. 2008;68:423–433.
29. Ruzsics B, Schwarz F, Schoepf UJ, et al. Comparison of dual-energy computed tomography of the heart with single photon emission computed tomography for assessment of coronary artery stenosis and of the myocardial blood supply. *Am J Cardiol*. 2009;104:318–326.
30. Cerqueira MD, Weissman NJ, Dilsizian V, et al. American heart association writing group on myocardial segmentation and registration for cardiac imaging. Standardized myocardial segmentation and nomenclature for tomographic imaging of the heart. A statement for healthcare professionals from the Cardiac Imaging Committee of the Council on Clinical Cardiology of the American Heart Association. *Int J Cardiovasc Imaging*. 2002;18:539–542.
31. Blankstein R, Shturman LD, Rogers IS, et al. Adenosine-induced stress myocardial perfusion imaging using dual-source cardiac computed tomography. *J Am Coll Cardiol*. 2009;54:1072–1084.
32. Stirrup J, Nicol E, Underwood SR. Defining myocardial infarction by cardiac computed tomography. *Int J Cardiovasc Imaging*. 2008;24:891–893.
33. Brodoefel H, Klumpp B, Reimann A, et al. Late myocardial enhancement assessed by 64-MSCT in reperfused porcine myocardial infarction: diagnostic accuracy of low-dose CT protocols in comparison with magnetic resonance imaging. *Eur Radiol*. 2007;17:475–483.
34. Baks T, Cademartiri F, Moelker AD, et al. Multislice computed tomography and magnetic resonance imaging for the assessment of reperfused acute myocardial infarction. *J Am Coll Cardiol*. 2006;48:144–152.
35. Gerber BL, Belge B, Legros GJ, et al. Characterization of acute and chronic myocardial infarcts by multidetector computed tomography: comparison with contrast-enhanced magnetic resonance. *Circulation*. 2006;113:823–833.
36. Lardo AC, Cordeiro MA, Silva C, et al. Contrast-enhanced multidetector computed tomography viability imaging after myocardial infarction: characterization of myocyte death, microvascular obstruction, and chronic scar. *Circulation*. 2006;113:394–404.
37. Baks T, Cademartiri F, Moelker AD, et al. Assessment of acute reperfused myocardial infarction with delayed enhancement 64-MDCT. *Am J Roentgenol*. 2007;188:W135–W137.
38. Hoffmann U, Millea R, Enzweiler C, et al. Acute myocardial infarction: contrast-enhanced multi-detector row CT in a porcine model. *Radiology*. 2004;231:697–701.